CAV2021
11th International Symposium on Cavitation
May 10-13, 2021, Daejon, Korea

Dynamics of the Re-entrant Jet in a Cavitating Venturi

Udhav U. Gawandalkar*, Christian Poelma

Multiphase Systems (Process & Energy), Mechanical, Maritime and Materials Engineering, Delft University of Technology, Leeghwaterstraat 21, 2628 CA Delft, The Netherlands

Abstract: Re-entrant jet initiated periodic cloud shedding is a well-known instability in partial cavitation. However, the exact physical mechanism governing it remains ambiguous. It is mainly due to experimental challenges in measuring it posed by the complicated topology of flow and limited optical access owing to opaque vapour clouds. We show that with fluorescent tracers and an optical filter, particle image velocimetry can be extended to measure re-entrant flow beneath the vapour cavity in an axisymmetric venturi. The whole-field, time-resolved velocity measurements of re-entrant flow (i) re-entrant flow velocity beneath attached cavities is not constant as it has a distinct variation in the axial direction, (ii) re-entrant flow velocity evolves both in space and time as the cavity grows, and (iii) the velocity of the re-entrant flow approaching the throat increases monotonically in time until the cavity develops a discontinuity.

Keywords: re-entrant jet; velocity measurement; Particle Image Velocimetry (PIV); cloud cavitation

1. Introduction

Partial cavitation occurs in a flow when low-pressure regions caused by separated shear layers get filled with vapours [1]. This phenomenon is inherently unsteady and leads to periodic shedding of clouds. The shed cavitation cloud can further implode violently near solid surfaces such as in ship propellers, pump impellers resulting in wear, noise and vibrations [2]. Hence, understanding the fundamentals of partial cavitation becomes imperative to mitigate the harmful effects associated with it.

Primarily two distinct mechanisms are responsible for periodic cloud shedding, depending on the cavitation number (σ) [3]: a re-entrant jet beneath the vapour cavity travelling in the direction opposite to bulk flow and a bubbly shock wave emanating from the previous cloud collapse. The re-entrant jet exists as a thin liquid film wedged in between the solid boundary and vapour cavity. The opacity of the vapour clouds results in poor optical access to the flow. Hence, it is cumbersome to experimentally study re-entrant flow and its dynamics. At present, the majority of the literature relies on the vapour cavity deformations by the re-entrant flow and space-time diagrams to estimate the re-entrant jet velocity [4, 5]. Some studies employ bubble tracking [5]. Moreover, single-point measurement techniques like optical or electrical impedance probes do not provide whole-field measurement, resulting in inadequate flow information.

It is reported that periodic cloud shedding is due to the adverse pressure-gradient driven re-entrant jet [6, 7]. However, a few studies maintain that the bubbly shock wave emanating from the previous cloud collapse in combination with the re-entrant jet triggers periodic cloud shedding [1, 5]. Consequently, there is no consensus on the exact physical mechanism driving such periodic cloud shedding. Hence, we present a time-resolved Particle Image Velocimetry (PIV) measurement of re-entrant flow in the near-wall region of a venturi using fluorescent tracer particles. The axisymmetry of venturi provides alternate/better optical access below the vapour cavity than in wedges [1] and hydrofoils [5]. The velocity measurements by PIV, complemented by high-speed photography, help to generate a better understanding of the dynamics of re-entrant jet initiated cloud shedding.

2. Experimental Methodology

* Corresponding Author: Udhav U. Gawandalkar, U.U.Gawandalkar@tudelft.nl

2.1. Flow facility

The experiments are performed in a cavitation loop at the Laboratory for Aero and Hydrodynamics in Delft with water as working fluid (see figure 1a). The partial cavitation occurs at the throat of the venturi made out of Poly(methyl methacrylate) (PMMA) with a divergence angle of 8° and throat diameter (d_t) of 16.66 mm as shown in figure 1b. The bulk flow rate is set to 2.2 liters/sec corresponding to $Re_t = 169700$ (the Reynolds number (Re_t) is defined on the throat diameter (d_t) and throat velocity (u_t)). Further, the global static pressure (P_0) is reduced to 45 kPa below ambient pressure using a vacuum pump. This allowed a cavitation number (σ) of 0.96, where periodic cloud shedding is re-entrant jet dominated. The shedding frequency is estimated using space-time diagrams to be 144 Hz, i.e. a Strouhal number defined on throat diameter (St_t) of 0.23. This value is in agreement with results from earlier studies [3].

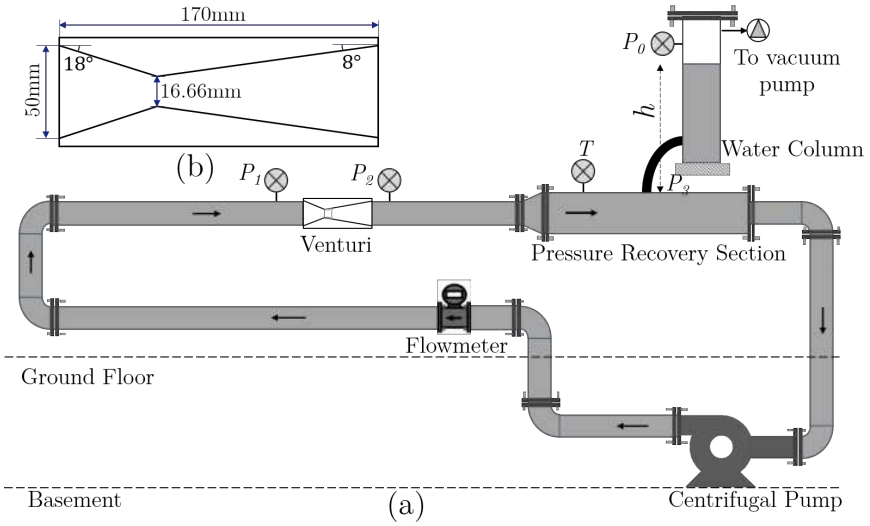

Figure 1. (a) Schematic of the cavitation loop. P_0, P_1, P_2, P_3 and T are pressure and temperature measuring stations respectively. (b) Axisymmetric venturi test section with geometric dimensions. Note that the arrows indicate flow direction.

2.2. Particle Image Velocimetry (PIV) setup

The planar PIV is employed to measure the velocity of the re-entrant jet in the near-wall region of the venturi (see figure 2a). The axisymmetry of the test section and vapour cavity is exploited to get an alternate

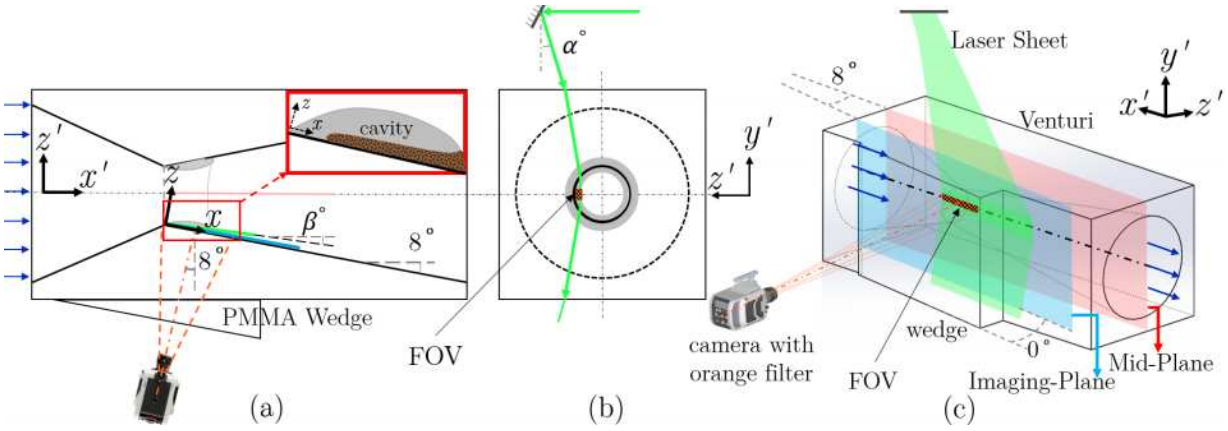

Figure 2. Schematics of PIV measurement setup in (a) x'-z' plane with inset showing zoom-in of vapour cavity and re-entrant flow beneath, (b) y'-z' plane, and (c) Isometric view showing imaging plane in blue and FOV in orange-black colour. Note that the bulk flow is left to right.

optical access to the re-entrant flow below the vapour cavity. Hence, a slender field of view (FOV) (~22×3.4 mm²) is selected to mitigate the effects of the curved wall (see figure 2c). The flow is seeded with fluorescent

* Corresponding Author: Udhav U. Gawandalkar, U.U.Gawandalkar@tudelft.nl

tracer particles made of acrylate resin coated with Rhodamine B. These particles, when illuminated with green light (λ~527 nm), emit orange light (λ~590 nm). A high-speed camera (Photron APX) is mounted at an angle of 8° w.r.t. z'-axis such that the camera sensor plane is parallel to the venturi wall (see figure 2a). A wedge of 8° made of PMMA is attached in front of the venturi to facilitate this (see figure 2c for the imaging plane shown in blue colour). The camera is equipped with an objective lens of 200 mm ($f^{\#} = 4$) and a high pass orange optical filter ($\lambda > 570$ nm). The use of fluorescent particles, in combination with a high-pass optical filter blocks the original green light, eliminating the bright reflections from the vapour cavity and test section. The light sheet generated by Nd:YLF laser (λ~527 nm) is introduced in the flow at an angle α°, β° w.r.t. y'-z', x'-z' respectively to illuminate re-entrant flow near the wall (see figure 2 a, b). The opaque vapour cavity beneath the flow serves as a knife-edge filter, thus illuminating only the particles in the thin liquid re-entrant film. A programmable timing unit (PTU) is used to synchronize high-speed laser and camera. A total of 15000 images are acquired at 18000 Hz. This frame rate ensured a suitable particle image displacement for PIV. An example of a raw image is shown in figure 3a.

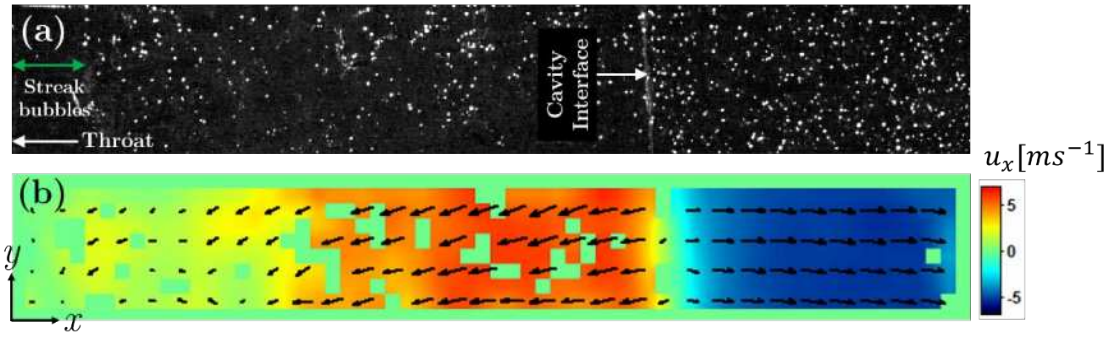

Figure 3. (a) A raw particle image with bright cavity interface and streak bubbles near the throat. (b) An instantaneous velocity vector field (every other vector is shown). The green voids represent outliers that have been removed. The bulk flow is from left to the right while re-entrant flow is from right to left.

The subsequent particle images are processed in DaVis 8.4. A multi-pass interrogation approach is followed wherein the interrogation window size is reduced from 48×48 pixels to 32×32 pixels (50% overlap). The vector fields are further post-processed by vector validation using universal outlier detection [8]. A sample post-processed velocity vector field is shown in figure 3b, where every other vector is shown for clarity.

2.3. Date Processsing: Selective Phase-Averaging Methodology

Since the cloud shedding phenomenon is quasi-periodic, a selective phase-averaging approach is used wherein the velocity data is averaged conditioned on a specific length of the cavity (l_c). For this, the space-time (x-t) diagram from the high-speed PIV images is used as a reference similar to Poelma et.al. [9]. Five attached cavity lengths in each cycle are selected, l_1-l_5: 10.2 mm, 10.7 mm, 11.7 mm, 12.7 mm, and 13.4 mm (see different colours in figure 4). Further, vertical lines corresponding to the above lengths ($l_{1,n}$-$l_{5,n}$) are plotted on the x-t diagram and their time of occurrence is noted on the time-axis (T) ($t_{1,n}$-$t_{5,n}$), where n corresponds to the rank of cycle (see figure 4). Finally, the velocity field for each

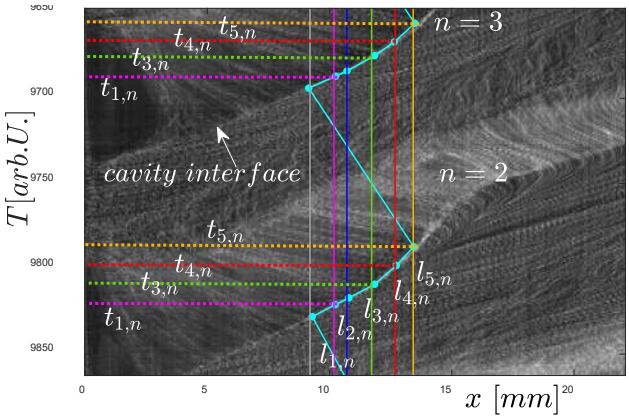

Figure 4. An x-t diagram showing phase-averaging approach for two shedding cycles. Each colour shows a different cavity length (l_1- l_5) and their time-stamp (t_1- t_5).

* Corresponding Author: Udhav U. Gawandalkar, U.U.Gawandalkar@tudelft.nl

cavity length (l_1-l_5) is averaged over 50 time-instances ($t_{i,1}$, $t_{i,2}$,.....$t_{i,50}$)$_{i=1,2,3,4,5}$ corresponding to 50 shedding cycles. The axial velocity (u_x) variation in the y-direction (see figure 3b) is neglected and u_x is further averaged in the y-direction to get only the axial (x) variation of $\overline{u_x}$.

3. Results

It is seen that as the vapour cavity grows beyond the streak bubbles (see figure 3a and x_b in figure 6b), the flow encounters a stagnation point at the cavity closure region and re-entrant flow is swept below the cavity. As the cavity grows further (l_1 to l_5), re-entrant flow continues to travel below the cavity, while the fluid on the other side of stagnation point moves away from the throat. This is evident from the change of

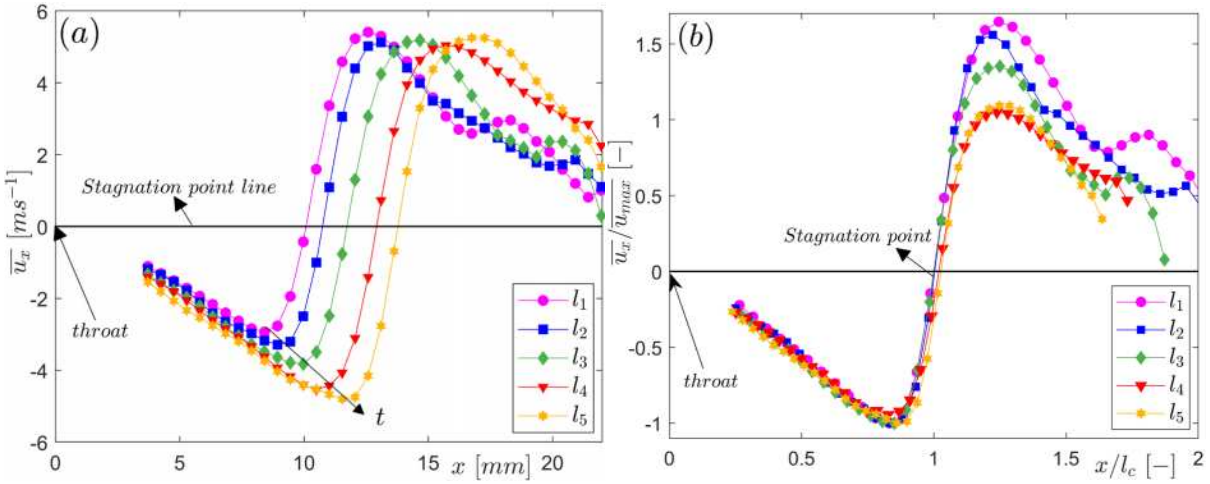

Figure 5. (a) Averaged axial velocity variation in axial direction in a single shedding cycle as vapour cavity grows from l_1 to l_5 in time t_1 to t_5. (b) Normalized velocity variation in axial direction where velocity is normalized by maximum velocity ($\overline{u_{max}}$) and x by cavity length (l_c). The re-entrant flow is shown by negative velocity.

velocity direction past the stagnation point in figure 5. As the re-entrant jet begins from the stagnation point, it accelerates towards the throat but at $x/l_c \sim 0.85$, starts slowing down (see figure 5b). This is because the flow is blocked by the streak type bubbles as clearly seen in the particle images (see figure 3a). Note that no tracer particles were imaged in the streak bubbles confirming the absence of a liquid film therein. Further, a jet with higher velocity is generated from the cavity closure point further away from the throat as evident from figure 5a. This is in agreement with the earlier observations [5] suggesting that re-entrant flow is a consequence of a stagnation point formed near the cavity closure point and adverse pressure gradient driving the reverse flow stream beneath the cavity. Moreover, as time progresses, the velocity of the re-entrant flow approaching the throat increases monotonically (see figure 5a) until the vapour cavity develops a discontinuity at $x \sim x_b$ (see also figure 6b). Thus, reinforcing that re-entrant jet initiates cloud detachment. This is followed by retraction of streak bubbles towards the throat and convection of detached cavitation cloud in the downstream region of the venturi. Interestingly, the averaged velocity ($\overline{u_x}$) when normalized with the peak velocity ($\overline{u_{max}}$) and axial distance (x) normalized with cavity length (l_c), collapse on top of each other showing self-similarity for re-entrant jet beneath the attached cavities (see figure 5b).

The PIV results can be interpreted as the average velocity of the fluid in the thin re-entrant jet film. Further insight can be obtained by investigating the velocity of the free cavity surface (see figure 6c). When re-entrant jet travels below the cavity, it deforms the free cavity surface, giving rise to upstream travelling structures. The velocity of these structures is estimated by performing cross-correlation on the high-speed images similar to PIV. Further, the velocity data is averaged using the phase-averaging methodology described in subsection 2.3. The axial variation of the axial-velocity ($\overline{u_x}$) was similar to observed in the

* Corresponding Author: Udhav U. Gawandalkar, U.U.Gawandalkar@tudelft.nl

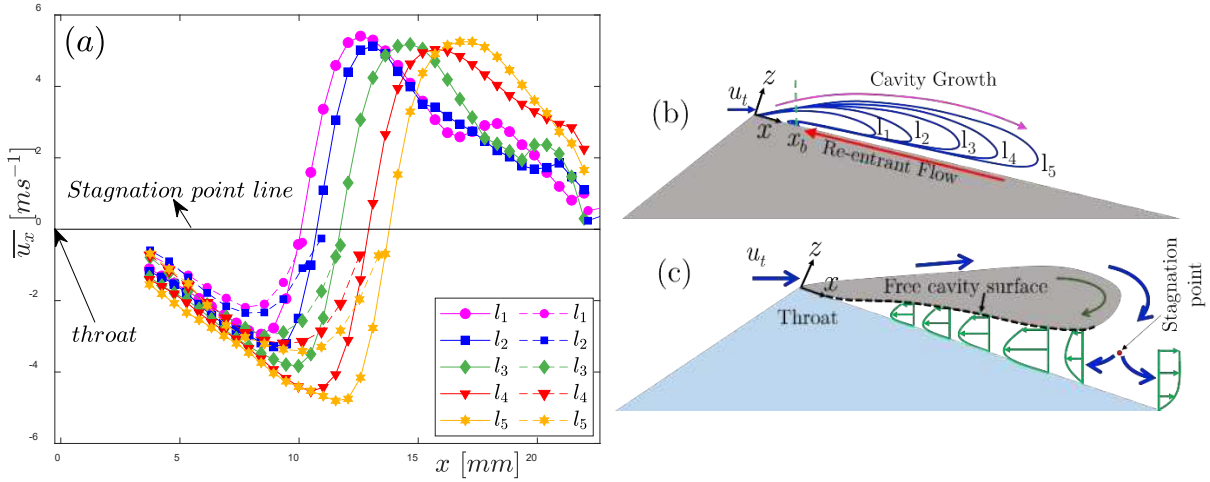

Figure 6. (a) The comparison of axial velocity variation on the cavity surface and liquid film at five different cavity growth stages (l_1-l_5). The solid lines correspond to re-entrant liquid film velocity while dashed lines correspond to cloud surface velocity (lower than in liquid film). (b) Schematic of cavity growth stages in a shedding cycle with x_b being spatial extent of streak bubbles. (c) Schematic of re-entrant jet flow with averaged velocity profiles.

liquid film for different cavity lengths. However, the magnitude of the velocity was 25% lower than in the liquid film (see dashed profiles in figure 6a). This is because flow close to the surface of the cavity is slowed down by the cavity growing in opposite direction. The whole-field velocity measurement of the re-entrant flow has shown that re-entrant flow evolves in both space and time as the vapour cavity grows (see figure 6a, b). Furthermore, it does not travel with constant velocity as reported before [4, 6] but has a distinct variation in the axial direction. In summary, the schematic of re-entrant flow emerges as shown in figure 6c. In the future, we also aim to estimate the *thickness* of the re-entrant jet film. This knowledge is required to fully describe the re-entrant flow and its dynamics.

Acknowledgments: UUG and CP have received funding from the ERC Consolidator Grant No. 725183 'OpaqueFlows'. The authors thank Edwin Overmars, Gertjan Mulder, Jasper Ruijgrok and Jan Graafland for their technical assistance.

References

[1] H. Ganesh, S. A. Makiharju, and S. L. Ceccio, "Bubbly shock propagation as a mechanism for sheet-to-cloud transition of partial cavities," *J. Fluid Mech.*, vol. 802, pp. 37–78, 2016.

[2] C. E. Brennen, *Cavitation and Bubble Dynamics*. Oxford University Press, 1995.

[3] S. Jahangir, W. Hogendoorn, and C. Poelma, "Dynamics of partial cavitation in an axisymmetric converging-diverging nozzle," *Int. J. Multiph. Flow*, vol. 106, pp. 34–45, 2018.

[4] M. Sakoda, R. Yakushiji, M. Maeda, and H. Yamaguchi, "Mechanism of cloud cavitation generation on a 2-D hydrofoil," in *Fourth International Symposium on Cavitation*, 2001, no. 1996, pp. 1–8.

[5] C. Stanley, T. Barber, and G. Rosengarten, "Re-entrant jet mechanism for periodic cavitation shedding in a cylindrical orifice," *Int. J. Heat Fluid Flow*, vol. 50, pp. 169–176, 2014.

[6] M. Callenaere, J. P. Franc, J. M. Michel, and M. Riondet, "The cavitation instability induced by the development of a re-entrant jet," *J. Fluid Mech.*, vol. 444, pp. 223–256, 2001.

[7] K. Laberteaux and S. Ceccio, "Partial cavity flows. Part 1. Cavities forming on models without spanwise variation," *J. Fluid Mech.*, vol. 431, pp. 1–41, 2001.

[8] J. Westerweel and F. Scarano, "Universal outlier detection for PIV data," *Exp. Fluids*, vol. 39, no. 6, pp. 1096–1100, 2005.

[9] C. Poelma, P. Vennemann, R. Lindken, and J. Westerweel, "In vivo blood flow and wall shear stress measurements in the vitelline network," *Exp. Fluids*, vol. 45, no. 4, pp. 703–713, 2008.

* Corresponding Author: Udhav U. Gawandalkar, U.U.Gawandalkar@tudelft.nl